Optimization of Medium Frequency Transformers with Practical Considerations

Kristen Booth*, Harish Subramanyan†, Xinyu Liang, Jun Liu†, Srdjan Srdic, and Srdjan Lukic
FREEDM Systems Center and †Department of Mechanical and Aerospace Engineering
North Carolina State University
Raleigh, North Carolina, USA
*kegarcia@ncsu.edu

***Abstract*—A method to design and optimize a Medium Frequency Transformer (MFT) based on commercially available components and semiconductor and converter constraints is presented. The optimization algorithm is used to redesign the transformer for a scaled-down electric vehicle (EV) fast charger using a three-level resonant circuit topology. The main consideration of this paper is the uncertainty caused by modeling assumptions in optimization algorithms. To reduce this uncertainty, space mapping is used to create an optimized design point. Finally, a comparison of the designs found using the original optimization algorithm and the space mapping technique are compared and analyzed. For simplicity, only a single objective optimization routine is employed.**

***Index Terms*—medium frequency, transformer, optimization, space mapping, electric vehicle, fast charger**

I. Introduction

Most grid-connected power electronic converters require a medium frequency transformer (MFT) for galvanic isolation. Some examples include Solid State Transformers (SSTs) [1]–[3], grid-tied inverters for photovoltaics [4], [5], auxiliary power supplies [6], and Electric Vehicle (EV) fast chargers [7]. However, the magnetics are often the bottleneck in designing highly efficient, power dense converters. In addition, the transformer parasitics are actively involved in resonant or dual-active bridge converter topologies to aid in zero voltage switching of the semiconductors [2], [3], [8].

Due to the limitations of the models used in the optimization algorithm, most optimization processes for MFTs ignore the realities of hardware design [9]–[12]. Ignoring these realities will only promote optimal designs that are not feasible in experimental setups. Therefore, it is imperative that power electronics design push toward optimization of realistic designs, including MFTs, that better correlate to the final hardware product.

Every analytical model for MFTs has some limitation as compared to the physical system. Leakage inductance calculations are based on a foil-type winding that fills the entire window height [13]. Core loss models assume that the flux density is uniform throughout the entire core [14]. Thermal models are currently designed in thermal isolation [15]; however, MFTs are in close proximity to other heat generating sources in the final experimental setup. While improvements to each of these models have been made to reach higher accuracy, the same limiting baseline assumptions remain.

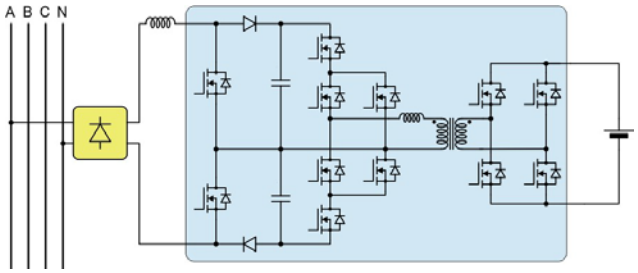

Fig. 1. Three-level LLC resonant converter with MFT.

TABLE I
Transformer Design Specifications

Design Variable	Rating
Input Voltage	600 V
Output Voltage	300 V
Rated Power	6.2 kW
Leakage Inductance (L_σ)	30-40 μH
Switching Frequency (f_{sw})	25-150 kHz

Research into modeling and parametric uncertainty for power electronic converters is limited. Reference [16] quantified these uncertainties but did not attempt to reduce them. This work aims to quantify and reduce modeling uncertainty in the design of an optimized MFT. The optimization routine is a single-objective Genetic Algorithm (GA), designed for maximum efficiency, to provide a simple discussion of the technique.

To reduce modeling uncertainty, Aggressive Space Mapping (ASM) will be used to reduce the model error [17]. This technique and the overall optimization algorithm is discussed in detail in Section II. Simulated results are presented in Section III. Finally, conclusions are discussed in Section IV.

II. Optimization Procedure

The MFT is being designed for a small-scale Electric Vehicle (EV) fast charger. The converter topology is a single-phase 3-level LLC resonant converter, shown in Fig. 1, and the design specifications for the MFT are given in Table I. The optimization algorithm, depicted in Fig. 2, incorporates an exterior GA with fitness derived through transformer

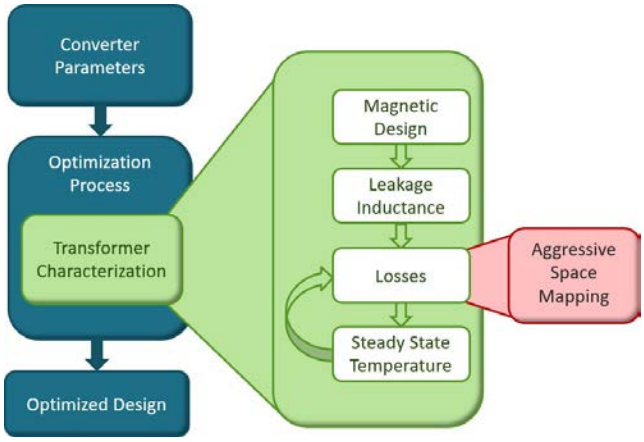

Fig. 2. Optimization algorithm for MFT.

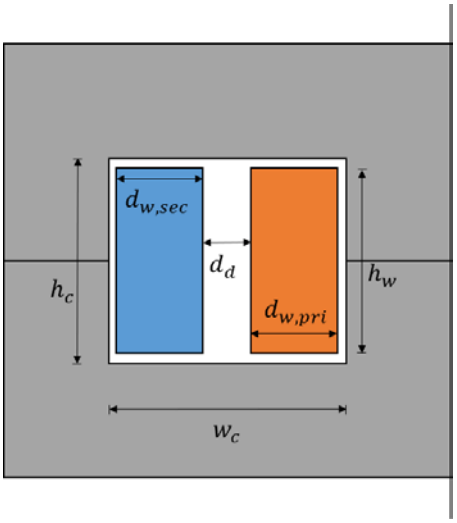

Fig. 3. Physical parameters for leakage inductance calculation.

characterization via analytical models. Finally, ASM is used to adjust the analytical models to higher fidelity models of Finite Element Analysis (FEA) to create a realistic final design for the hardware. The rest of this section is devoted to discussing the details of the transformer characterization and space mapping.

The initial magnetics design is created using the conventional methods, as discussed in [18], before the other calculations can take place. In order to reduce computational effort, any unfeasible designs are removed after each step within the transformer characterization process.

A. Leakage Inductance

The leakage inductance, L_σ, is calculated using the methods described in [19]. The physical parameters required can be found in Fig. 3. For Litz wire, the porosity factor can be calculated as

$$\eta = \frac{N_{sv}\, d_{eq}}{h_{core}} \tag{1}$$

where $d_{eq} = \sqrt{\pi/4}\, d_r$. Due to the nonuniform structure of Litz winding, the number of windings oriented horizontally, N_{sh}, or vertically, N_{sv}, can be calculated based on the proportional assumption that the total winding cross-sectional profile is followed by the individual strands as

$$K_w = \frac{h_w}{d_{eq}}. \tag{2}$$

Thereby the horizontal and vertical number of windings can be calculated in (3) and (4), respectively, where N_s is the number of strands in the Litz wire.

$$N_{sh} = \sqrt{\frac{N_s}{K_w}} \tag{3}$$

$$N_{sv} = \sqrt{K_w N_s} \tag{4}$$

The Rogowski factor adjusts the equivalent length of the magnetic flux and can be calculated as

$$K_R = 1 - \frac{1 - e^{-\pi h_w/(d_{w,pri} + d_d + d_{w,sec})}}{\pi h_w/(d_{w,pri} + d_d + d_{w,sec})} \tag{5}$$

which creates the improved height,

$$h_{eq} = \frac{h_w}{K_R}. \tag{6}$$

Therefore, the modified Dowell's method to include these modifications is

$$L_\sigma = \mu_0 N_{pri}^2 \frac{l_T}{h_{eq}} \left[\frac{d_{eq,pri} N_{sh}}{3} F_{w,pri} + \frac{d_{eq,sec} N_{sh}}{3} F_{w,sec} + d_d + d_{wi,pri} \frac{(N_{sh}-1)(2N_{sh}-1)}{6N_{sh}} + d_{wi,sec} \frac{(N_{sh}-1)(2N_{sh}-1)}{6N_{sh}} \right] \tag{7}$$

where

$$F_{w,y} = \frac{1}{2N_{sh}^2 \Delta} \left[(4N_{sh}^2 - 1)\phi_1 - 2(N_{sh}^2 - 1)\phi_2 \right], \tag{8}$$

$$\phi_1 = \frac{\sinh(2\Delta) - \sin(2\Delta)}{\cosh(2\Delta) - \cos(2\Delta)} \tag{9}$$

$$\phi_2 = \frac{\sinh(\Delta) - \sin(\Delta)}{\cosh(\Delta) - \cos(\Delta)} \tag{10}$$

$$\delta = \sqrt{\frac{1}{\pi \mu_0 \eta \sigma f_{sw}}} \tag{11}$$

N_{pri} is the number of primary winding turns, $\Delta = d_{eq}/\delta$, l_t is the mean turn length, d_d is the gap between the primary and secondary windings, $d_{w,y}$ is the equivalent winding width, and $d_{wi,y}$ is the width of the dielectric between layers.

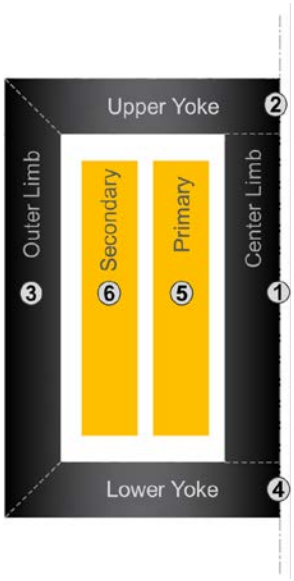

Fig. 4. Two dimensional physical layout of thermal model.

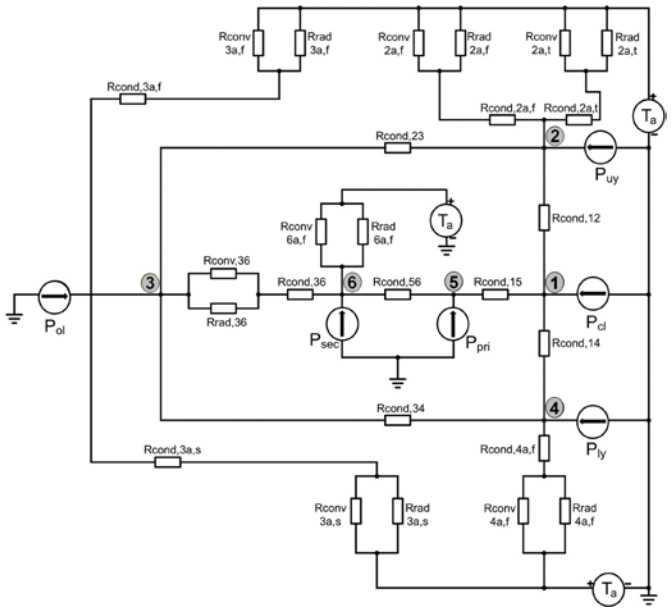

Fig. 5. Thermal resistive network for MFT design.

B. Winding Losses

Dowell's method is the most commonly used method for generically calculating winding losses in MFTs [13]. However, this optimization is based on a specific Litz wire, so the manufacturer's method is used as described in [20]. The winding losses for Litz wire can be determined using

$$R_{DC} = \frac{R_s (1.015)^{N_B} (1.025)^{N_C}}{N_S} \tag{12}$$

and

$$R_{AC} = \sum H + K \cdot \frac{N_S \times D_I}{D_O}^{2} \sum \sum tt \; R_{DC} \tag{13}$$

where R_{DC} is DC resistance [Ω/1000ft], R_S is the maximum DC resistance, R_{AC} is AC resistance [Ω/1000ft], D_I is the individual strand diameter [in], and D_O is entire cable diameter [in]. N_B is the bunching operations number, N_C is the cabling operations number, $\sum N_S$ is the number of individual strands, and $tt = \frac{D \sqrt{f} * 1000}{10.44}$. H and K are given by the manufacturer.

C. Core Losses

The improved General Steinmetz Equation (iGSE) is most commonly used to calculated core losses for MFT optimization algorithms [14]. iGSE is defined as

$$P_c = \frac{1}{T} \int_0^T k_i \left| \frac{dB(t)}{dt} \right|^{\alpha} (\Delta B)^{\beta - \alpha} dt \tag{14}$$

where

$$k_i = \frac{K}{(2\pi)^{\alpha - 1} \int_0^{2\pi} |\cos\theta|^{\alpha} 2^{\beta - \alpha} d\theta}, \tag{15}$$

K, α, and β are given by the manufacturer. iGSE is the most widely used core loss empirical method for MFTs as it reduces to a simple equation for square wave excitation found in MF converters. As K is dependent on the core temperature, an iterative process between the core losses and thermal occurs until equilibrium is reached. For simplicity, the manufacturer's core loss calculation is used in this optimization algorithm for the Ferroxcube 3C90 material.

D. Thermal Modeling

The core and winding losses lead to an increase in the operating temperature of the transformer which makes it imperative to calculate the hot-spot. A 2D analytical model is employed which is a simplified version found in [15]. It is then validated using 3D FEA analysis in order to confirm the hot-spot locations.

The core is divided into four zones: Upper Yoke, Lower Yoke, Center Limb, and Outer Limb, as shown in Fig. 4. The core losses from each of the zones are modeled as heat sources which are directly proportional to the volume of the corresponding zone. The heat is exchanged between the cores and windings by conduction and radiation. The heat is then lost to the surrounding atmosphere by natural convection and radiation from the front, back, top, and sides of the transformer. It is assumed that the bottom surface of the transformer core is perfectly insulated. This most closely represents the MFT being directly mounted to a surface which will be the case in the experimental setup. The primary and secondary windings are represented using two zones inside the core window.

The well-known electrical circuit analogy is used to couple these six zones where different heat transfer mechanisms are characterized by thermal resistances.

The conduction resistance is defined as

$$R_{cond} = \frac{L}{kA} \tag{16}$$

where k is the thermal conductivity, A is the cross-sectional area, and L is the length of conduction path.

The convection resistance can be calculated using

$$R_{conv} = \frac{1}{h_{conv} A} \tag{17}$$

where

$$h_{conv} = \frac{Nu \cdot k}{L_c}, \tag{18}$$

N u is the Nusselt number, L_c is the characteristic length, and k is the thermal conductivity of air at the mean film temperature. The Nusselt number was calculated under the assumption that the heat loss from the transformer is equivalent to convection over a hot-plate.

The radiation resistance is given by

$$R_{rad} = \frac{1}{h_{rad} A} \tag{19}$$

where

$$h_{rad} = \sigma s \frac{T_1^4 - T_2^4}{T_1 - T_2}, \tag{20}$$

σ is the Stefan-Boltzmann constant, and s is the emissivity.

A detailed resistance network is shown in Fig. 5. The admittance matrix, Y , was derived using the six nodal points which were selected to best reflect the temperature profile across the transformer. The temperatures at the respective nodes can be obtained using

$$Q = Y \Delta T \tag{21}$$

where Q is the heat loss and ΔT is the temperature matrix. Nodes 4 and 6 are expected to be the hot-spots for the core and winding respectively due to the nature of their locations in the resistance network and the power loss generated by the individual components of the MFT.

E. Aggressive Space Mapping for MFT Optimization

The basic approach of ASM is to calibrate a coarse (analytical) model to a fine (FEA) model to accelerate design optimization. ASM starts with the optimization argument

$$\mathbf{x}^* = \arg\min_{\mathbf{x}^*} U(\mathbf{R}(\mathbf{x})), \tag{22}$$

where $\mathbf{R} \in \mathrm{IR}^{m\times 1}$ is a vector of m responses of the model, $\mathbf{x}$ is the vector of n design parameters, and U is the objective function. $\mathbf{x}^*$ is the unique optimal solution to be determined.

The fundamental component of SM is that the coarse model and fine model $\mathbf{x}_c$ and $\mathbf{x}_f \in \mathrm{IR}^{n\times 1}$, respectively, can be mapped, **P**, as

$$\mathbf{x}_c = \mathbf{P}(\mathbf{x}_f) \tag{23}$$

such that

$$\mathbf{R}_c(\mathbf{P}(\mathbf{x}_f)) \approx \mathbf{R}_f(\mathbf{x}_f) \tag{24}$$

in a region of interest where $\mathbf{R}_c$ and $\mathbf{R}_f \in \mathrm{IR}^{m\times 1}$ are the corresponding response vectors.

As $\mathbf{R}_f(\mathbf{x}_f^{j+1})$ goes to $\mathbf{R}_c(\mathbf{x}_c)$, then $\mathbf{x}_c^{j+1} = \mathbf{P}(\mathbf{x}_f^{j+1})$ approaches $\mathbf{x}_c^*$ as the iteration number reaches a final converging iteration, M ,

$$\|\mathbf{x}_c^{j+1} - \mathbf{x}^*\| \le \eta \quad \text{as } j \to M \tag{25}$$

where η is a small tolerance. The goal of ASM is to set $\eta = 0$ in (25). This creates a set of n nonlinear equations to be set to zero,

$$\mathbf{f} = \mathbf{f}(\mathbf{x}_f) = \mathbf{P}(\mathbf{x}_f) - \mathbf{x}_c^* = 0. \tag{26}$$

Let $\mathbf{x}_f^{(j)}$ be the jth iteration to the solution of (26) and $\mathbf{f}^{(j)}$ stand for $\mathbf{f}(\mathbf{x}_f^{(j)})$. The next iteration can be found by a quasi-Newton method

$$\mathbf{x}_f^{(j+1)} = \mathbf{x}_f^{(j)} + \mathbf{h}^{(j)} \tag{27}$$

where **h** is the solution to

$$\mathbf{B}^{(j)}\mathbf{h}^{(j)} = -\mathbf{f}^{(j)} \tag{28}$$

and **B** is an approximation to the Jacobian matrix. For the first iteration, $\mathbf{B}^{(1)}$ is the identity matrix. For every iteration following, **B** is updated by the Broyden formula which can be reduced to

$$\mathbf{B}^{(j+1)} = \mathbf{B}^{(j)} + \frac{\mathbf{f}^{(j+1)}\mathbf{h}^{(j)T}}{\mathbf{h}^{(j)T}\mathbf{h}^{(j)}}. \tag{29}$$

The algorithm is complete when

$$\|\mathbf{f}^{(j+1)}\| \le \eta. \tag{30}$$

ASM enables speed within the global design space optimization while improving the accuracy of the optimal design using the fine model. Discussion of the impacts of this technique are provided in Section III.

TABLE II
OPTIMIZED TRANSFORMER DESIGNS

	SOA Design	**ASM Design**
Primary Turns	12	10
Core Sets	6	6
f_{SW} (kHz)	150	125
Analytical Core Loss (W)	4.3	-
FEA Core Loss (W)	3.5	4.4
Total Losses (W)	15.1	13.3

III. SIMULATED RESULTS

Using the optimization algorithm without and with ASM, the two resulting designs are described and compared. It is important to note that the only design objective is maximizing efficiency; however, multiobjective optimization would render a similar comparison with two differing designs. Both designs are given in Table II for this comparison.

The State of the Art (SOA) design uses only the first two stages of the optimization algorithm in Fig. 2 while the ASM design extends the optimization until the modeled design is properly mapped to the fine model. This extension of the optimization process procures a design that is in better

agreement with the FEA output which, in turn, should make the experimental outputs more similar to the expected response of the optimal modeled design than in previous work.

ASM occurs through the core loss calculations. The core losses are space mapped while the winding losses are calculated using the analytical model discussed in Section II. ASM is considered complete when the difference between the core loss in the analytical model and FEA is less than 0.2 W. This process took two iterations of ASM.

The losses, shown in Table II, are the core losses of each design via the coarse and fine models. It can be seen that the ASM technique puts the core loss of the ASM design within the accepted tolerance limit. While this particular optimization routine does not show a large difference in the core loss between the two designs, it can be assumed that this response difference may increase with more optimization objectives or a larger power rating of the system. This difference is vital to larger systems that require extremely high converter efficiency, such as SSTs or EV fast chargers.

While the overall size of the MFT is relatively unchanged, there is a reduction in the number of turns and switching frequency which reduces the overall losses, shown in the last row of Table II. This also lowers the expected temperature of the MFT. A comparison of the expected temperatures is given in Table III. Therefore, the feasible region of MFT designs for power density using the ASM technique will also be affected by the design adjustment as the temperature of the transformer is dependent upon the losses.

TABLE III
TRANSFORMER ESTIMATED TEMPERATURES IN DEGREES CELSIUS

Node	SOA Design	ASM Design
1	76.4	70.5
2	60.3	56.7
3	55.7	52.7
4	71.5	66.6
5	80.1	73.1
6	82.8	75.7

The final design used in the FEA of the MFT is depicted in Fig. 6. Since the thermal model and the leakage inductance calculation assume a full layer, the secondary winding layer is assumed to be complete. This is a baseline assumption that inhibits the modeling of the MFTs. This is a source of modeling error that cannot be removed.

IV. CONCLUSIONS

This work aims to discuss the limitations of analytical optimization algorithms and improve upon them using ASM. The simulated results of these two algorithms using a single objective example are given and compared. It is shown that two of the three design variables are updated through the ASM technique. Therefore, it can be concluded that using ASM, or a similar technique, is relevant and necessary for building the most optimal design possible.

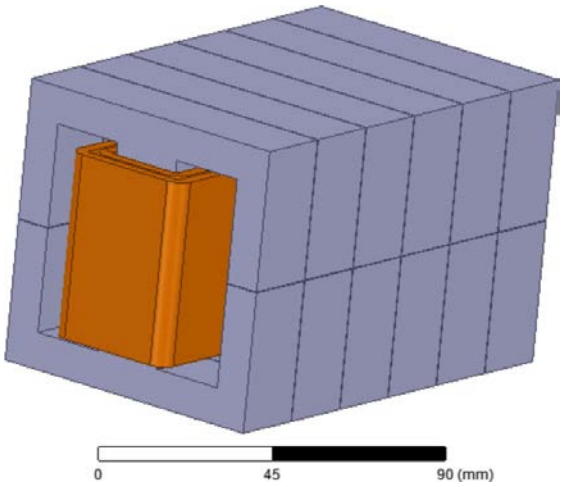

Fig. 6. FEA model of MFT.

Future work entails building and comparing the two designs in the experimental setup of the small-scale EV fast charger converter for verification. To further the research into this updated optimization algorithm, a multiobjective optimization algorithm will be employed that will include leakage inductance and power density to see the effects of this method on a larger scale. This background is also enlightening for sensitivity analysis of MFT designs for use in a robust optimization algorithm by incorporating manufacturing tolerances into the overall algorithm.

ACKNOWLEDGEMENTS

This material is based upon work supported by the National Science Foundation under Grant No. DGE-1252376. Kristen Booth would like to acknowledge John Bandler for his guidance through the space mapping technique.

REFERENCES

[1]X. She, A. Q. Huang, and R. Burgos, "Review of Solid-State transformer technologies and their application in power distribution systems," *IEEE Journal of Emerging and Selected Topics in Power Electronics*, vol. 1, no. 3, pp. 186–198, 2013.

[2]G. Ortiz, M. Leibl, J. W. Kolar, and O. Apeldoorn, "Medium frequency transformers for solid-state-transformer applications — design and experimental verification," in *2013 IEEE 10th International Conference on Power Electronics and Drive Systems (PEDS)*, Apr. 2013, pp. 1285–1290.

[3]J. E. Huber, J. B öhler, D. Rothmund, and J. W. Kolar, "Analysis and cell-level experimental verification of a 25 kw all-SiC isolated front end 6.6 kv/400 V AC-DC solid-state transformer," *CPSS Transactions on Power Electronics and Applications*, vol. 2, no. 2, pp. 140–148, 2017.

[4]F. V. Amaral, T. M. Parreiras, G. C. Lobato, A. A. P. Machado, I. A. Pires, and B. de Jesus Cardoso Filho, "Operation of a Grid-Tied cascaded multilevel converter based on a forward Solid-State transformer under unbalanced PV power generation," *IEEE Trans. Ind. Appl.*, vol. 54, no. 5, pp. 5493–5503, 2018.

[5]S. Kouro, J. I. Leon, D. Vinnikov, and L. G. Franquelo, "Grid-Connected photovoltaic systems: An overview of recent research and emerging PV converter technology," *IEEE Ind. Electron. Mag.*, vol. 9, no. 1, pp. 47–61, Mar. 2015.

[6]D. Peftitsis, M. Antivachis, and J. Biela, "Auxiliary power supply for medium-voltage modular multilevel converters," in *2015 17th European Conference on Power Electronics and Applications (EPE'15 ECCE-Europe)*, 2015, pp. 1–11.

[7]S. Srdic, X. Liang, C. Zhang, W. Yu, and S. Lukic, "A SiC-based high-performance medium-voltage fast charger for plug-in electric vehicles," in *2016 IEEE Energy Conversion Congress and Exposition (ECCE)*, 2016, pp. 1–6.

[8]M. A. Bahmani, T. Thiringer, and M. Kharezy, "Design methodology and optimization of a medium frequency transformer for high power DC-DC applications," in *2015 IEEE Applied Power Electronics Conference and Exposition (APEC)*, Mar. 2015, pp. 2532–2539.

[9]J. W. Kolar, J. Biela, S. Waffler, T. Friedli, and U. Badstuebner, "Performance trends and limitations of power electronic systems," in *2010 6th International Conference on Integrated Power Electronics Systems*, Mar. 2010, pp. 1–20.

[10]I. Villar, "Multiphysical characterization of Medium-Frequency power electronic transformers," Ph.D. dissertation, ETH Zurich, 2010.

[11]G. Ortiz, J. Biela, and J. W. Kolar, "Optimized design of medium frequency transformers with high isolation requirements," in *IECON 2010 - 36th Annual Conference on IEEE Industrial Electronics Society*, Nov. 2010, pp. 631–638.

[12]M. Mogorovic and D. Dujic, "100kw, 10khz medium frequency transformer design optimization and experimental verification," *IEEE Trans. Power Electron.*, pp. 1–1, 2018.

[13]P. L. Dowell, "Effects of eddy currents in transformer windings," *Electrical Engineers, Proceedings of the Institution of*, vol. 113, no. 8, pp. 1387–1394, Aug. 1966.

[14]K. Venkatachalam, C. R. Sullivan, T. Abdallah, and H. Tacca, "Accurate prediction of ferrite core loss with nonsinusoidal waveforms using only steinmetz parameters," in *2002 IEEE Workshop on Computers in Power Electronics, 2002. Proceedings.*, Jun. 2002, pp. 36–41.

[15]M. Mogorovic and D. Dujic, "Thermal modeling and experimental verification of an air cooled medium frequency transformer," in *2017 19th European Conference on Power Electronics and Applications (EPE'17 ECCE Europe)*, 2017, pp. P.1–P.9.

[16]N. R. Mehrabadi, R. Burgos, C. Roy, and D. Boroyevich, "Power electronics modeling and design: Using parametric and Model-Form uncertainty quantification to assess predictive accuracy of power converter models," *IEEE Power Electronics Magazine*, vol. 4, no. 4, pp. 44–52, Dec. 2017.

[17]J. W. Bandler, R. M. Biernacki, S. H. Chen, R. H. Hemmers, and K. Madsen, "Electromagnetic optimization exploiting aggressive space mapping," *IEEE Trans. Microw. Theory Tech.*, vol. 43, no. 12, pp. 2874–2882, Dec. 1995.

[18]R. W. Erickson and D. Maksimovic, *Fundamentals of Power Electronics*, 2nd ed. Springer, 2001.

[19]M. Mogorovic and D. Dujic, "Medium frequency transformer leakage inductance modeling and experimental verification," in *2017 IEEE Energy Conversion Congress and Exposition (ECCE)*, Oct. 2017, pp. 419–424.

[20]"New England Wire," http://www.litzwire.com/nepdfs/Litz Technical.pdf, accessed: 2018-02-15.